Pergamon

Engineering Fracture Mechanics Vol. 54, No. 4, pp. 457–470, 1996

0013-7944(95)00242-1
0013-7944/96 $15.00 + 0.00

SOME STUDIES ON THE INFLUENCE OF STRESS RATIO AND TEST TEMPERATURE ON X-RAY FRACTOGRAPHY OBSERVATIONS IN C45 STEEL SPECIMENS†

K. RAJANNA

Metallurgy Department, Corporate R&D Division, B.H.E.L., Vikas Nagar, Hyderabad-500 593, India

B. PATHIRAJ and B. H. KOLSTER

Faculty of Mechanical Engineering, University of Twente, 7500 AE Enschede, The Netherlands

Abstract—This paper deals with additional "X-ray fractography" observations made on C45 steel, subsequent to the earlier work [K. Rajanna, B. Pathiraj and B. H. Kolster, Fatigue fracture surface analysis in C45 steel specimens using X-ray fractography. *Engng Fracture Mech.* **39**, 147–157 (1991)]. Fatigue crack growth tests were carried out at 20°C on CT samples prepared from this steel using different stress ratios (0.1R, 0.5R and 0.7R). Tests were also carried out at different temperatures (− 20°C, 20°C and 115°C) using a stress ratio of 0.1. The fractured surfaces were analysed for their residual stress state. The influence of the test conditions on the residual stresses developed is discussed. Copyright © 1996 Elsevier Science Ltd.

1. INTRODUCTION

THE METHOD to analyse fracture surfaces using X-ray diffraction is known as "X-ray fractography" [1]. In this method, the measured residual stress (σ_r) and the Full Width at Half Maximum (FWHM, denoted by "B") are correlated to the fracture mechanics parameters such as maximum stress intensity factor (K_{max}), stress intensity factor range (ΔK) or fracture toughness (K_{Ic}). The method was employed by many investigators to analyse the fracture mechanisms in a specimen tested for fatigue crack growth rate [2–6] of different materials. In all these investigations, tensile residual stresses were observed at the fracture surface. Different trends were noticed in the variation of σ_r with K_{max} or ΔK. These include: a monotonic increase [7], a monotonic decrease [8] and an increase followed by a decrease [2, 3, 9].

In general, the magnitude of σ_r is found to increase with increasing stress ratio "R", particularly in the lower ΔK region [2]. Different results show that R-ratio has an influence on the $\sigma_r - K_{max}$ relation, but not on the $\sigma_r - \Delta K$ relation [10]. However, there are other reports showing the influence of R-ratio to be confined to $\sigma_r - \Delta K$ but not to $\sigma_r - K_{max}$ [7]. With regard to the relation of B with K_{max} or ΔK, in a few cases it is found to be more dependent on monotonic loading (K_{max}) rather than on cyclic loading (ΔK) [2, 11] while in some other cases B is found to be influenced by R-ratio [12]. These observations suggest that the $\sigma_r - K_{max}$ (ΔK) or $B - K_{max}$ (ΔK) relationships are dependent on the material and its response to cyclic loading (strain hardening behaviour).

More encouraging results have been reported by many investigators from sub-surface X-ray analysis. The most promising application of this method is found in the determination of the monotonic plastic zone size, r_p. It was found that the r_p values determined through the sub-surface X-ray analysis at different locations on the fracture surface are in good agreement with the predicted r_p values according to the relationship given below.

$$r_p = \alpha\left[\frac{K_{max}}{\sigma_{ys}}\right]^2. \tag{1}$$

In most of these investigations, a linear relationship was reported between the r_p values obtained from X-ray sub-surface analysis and $(K_{max}/\sigma_{ys})^2$, whose slope was found to be the same

†This research work was carried out at The Foundation for Advanced Metals Science (SGM), Hengelo, The Netherlands where the authors were working earlier.

as the one determined by finite element analysis ($\alpha = 0.15$) [13]. However, in some cases differences were noticed in slopes from the theoretical "α" value. These differences were attributed to the differences in σ_{ys} as a consequence of fatigue cycling effects (cyclic softening or hardening behaviour).

In sub-surface X-ray analysis, an increase in the level of residual stresses (σ_r) with depth has been observed by several investigators. The depth at which the peak stress is observed was found to increase with K_{max} or ΔK. This led to a conclusion [14] that the depth could be related to the reverse plastic zone size, r_{pc}, within which the material is plastically deformed in tension and compression during each load cycle. Some others have also attempted [15] to provide an explanation along similar lines for different trends observed in the distributions of σ_r and B as a function of depth below the fracture surface. A reasonably good agreement was seen between the theoretically predicted and experimentally obtained r_{pc} values. The reverse plastic zone, r_{pc}, for different ΔK is calculated using the following equation:

$$r_{pc} = \alpha\left[\frac{\Delta K}{\sigma_{ys}'}\right]^2. \tag{2}$$

In the above eqs (1) and (2) σ_{ys} and σ_{ys}' represent the yield stress values in monotonic and cyclic loading conditions.

Bignonnet *et al.* [16] have observed a plateau region in the σ_r distribution in the presence of a lower stress ratio. They explain that this plateau was caused mainly by crack closure. In some other investigations [2], the relationship between the r_{pc} and σ_r distributions was not clear. In these cases, the peaks in the σ_r distribution were observed at a depth which was found to be the same as the roughness of the fracture surface. As a result the depth at which peaks were observed was attributed to the roughness of the fracture surface. The observed low residual stress at the fracture surface was attributed [9] to the stress relief caused by the roughness of the fractured surfaces.

From the above discussions it may be noted that though several explanations have been offered for an increase in σ_r below the fracture surface, an unequivocal explanation is still not available. In an attempt to provide a reasonable explanation for the different trends observed in the distributions of σ_r and B with K_{max} as well as the depth, detailed studies were carried out on fatigue fracture surfaces of C45 steel in different heat treated conditions, austenitic stainless and duplex steels [17]. The present investigation studies the influence of stress ratio (greater than $0.1R$) and the test temperature on X-ray fractography results, in particular the σ_r and B variations with K_{max} and the depth below fracture surface in a C45 steel.

2. MATERIAL AND EXPERIMENTAL PROCEDURES

2.1. *Material*

A hot rolled medium carbon structural steel of C45 grade was selected in this investigation. The chemical composition of the steel is shown in Table 1. Blanks of suitable dimensions were cut from the stock material in order to prepare different test specimens. These were solutionised at 850°C for 1 hr and subsequently water quenched. Thereafter, they were subjected to a tempering treatment at 600°C for 2 hrs.

2.2. *Specimen preparation details*

Flat samples with 10 mm × 7 mm cross section and 50 mm gauge length were prepared for determining the tensile properties. 15 mm thick Compact Tension Specimens (CTS) were prepared according to the ASTM E-647 standard for fatigue crack growth tests. Machine notches were made in CT specimens using spark erosion technique with the notch length coinciding with the rolling direction. The notch lengths were made to correspond to 0.3 crack length-to-width ratio (a/w).

Table 1. Chemical composition (weight %) of the steel investigated

C	Mn	Si	S
0.44	0.64	0.23	0.032

Table 2. Room temperature tensile properties

0.2% Yield strength	630 MPa
Ultimate tensile strength	720 MPa
Elongation (25 mm G.L.)	18.0%

2.3. *Experimental procedures*

An electro-mechanical test system of 250 kN capacity (Schenck Trebel RM 250 type) was employed to perform the tensile tests at room temperature according to the DIN 50145 standard and the results are shown in Table 2.

All fatigue crack growth tests were conducted on a 100 kN universal static/dynamic MTS servo hydraulic test system, following the procedure described in ASTM E-647 standard. The tests were performed at room temperature (20°C) using 0.1, 0.5 and 0.7 R-ratios and at -20, 20 and 115°C temperatures using 0.1 R-ratio. Fatigue crack growth rate test results are presented in the normal log (da/dN) vs log (ΔK) plots in Fig. 1 for the tests performed at different stress ratios and in Fig. 2 for the tests performed at different temperatures. The determined Paris constants for stage II region of tests performed using different R ratios and different temperatures are shown in Tables 3 and 4, respectively. The values of "m" for different stress ratios and for different temperatures indicate that the crack growth rate decreases with increasing temperature and increases with increasing stress ratio.

2.4. *X-ray analysis*

X-ray analysis of the fatigue fractured surfaces of the specimens was performed using the multiple exposure $\sin^2\psi$ method [18]. A portable X-ray stress analyser Rigaku strainflex MSF-2M was employed for this purpose. All X-ray studies were carried out using {211} reflection and Cr K_α radiation. The X-ray irradiated area was restricted to a strip of 10 mm in length and about 1 mm in width. The measurements were performed in the direction of crack growth and at different crack locations which correspond to different K_{max} or ΔK values. The sub-surface stress distribution was determined from measurements made after removing layers of material by electropolishing.

3. RESULTS AND DISCUSSION

3.1. *Fracture surface analysis*

The distributions of the measured residual stress (σ_r) as well as the FWHM (B) of the diffraction profile (at $\psi = 0$ deg.), as a function of K_{max} are shown in Figs 3 and 4, respectively,

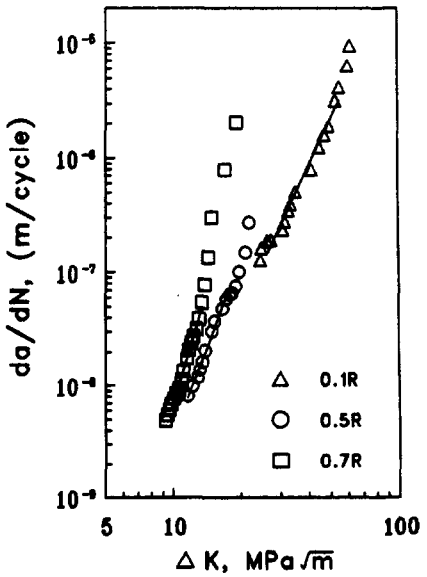

Fig. 1. Log (da/dN) vs Log ΔK plots for tests performed using different R-ratios.

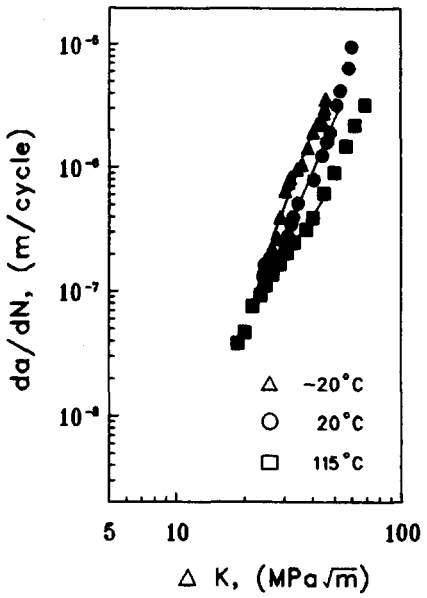

Fig. 2. Log (da/dN) vs Log ΔK plots for tests performed using different temperatures.

for the fatigue crack growth tests performed at 20°C using 0.1R, 0.5R and 0.7R. For tests performed at -20, 20 and 115°C using a 0.1R, the variation of σ_r and B as a function of K_{max} are shown in Figs 5 and 6, respectively.

3.1.1. *X-ray analysis of the fractured surfaces of specimens tested using different stress ratios.* The $\sigma_r - K_{max}$ relationship for 0.7R test condition (Fig. 3) exhibits a monotonically decreasing trend while for 0.1R and 0.5R test conditions exhibit an increase to a maximum followed by a decrease. In the initial stages (up to a K_{max} value of about 60 MPa$\sqrt{m}$), the σ_r values are larger for 0.7R and lower for 0.1R test conditions. This observation is in agreement with the result of an elasto-plastic finite element analysis [2] in predicting the magnitude of σ_r at the fracture surface and its variation as a function of stress ratio. Beyond 60 MPa $\sqrt{m}$ the trends are opposite in nature. The maximum value of σ_r is *ca* 250 MPa for 0.1 and 0.5R test conditions. However, the K_{max} at which this maximum occurs shifts to a lower level for tests performed using higher stress ratios. For 0.7R a maximum σ_r value of *ca* 325 MPa is seen in the initial stages of crack growth itself (Fig. 3).

Changes in FWHM (B) as a function of K_{max} (Fig. 4) show a gradual increase for 0.1 and 0.5R test conditions. For 0.7R the variation is marginal in the stable crack growth fatigue region (up to *ca* 70 MPa$\sqrt{m}$). Beyond a K_{max} value of about 80 MPa$\sqrt{m}$, the B variations show a sharply increasing trend. In general, the B values at any K_{max} are larger for 0.7R than those for the other stress ratios.

3.1.2. *X-ray analysis of the fractured surfaces of specimens tested using different test temperatures.* The distribution of σ_r with K_{max} at -20°C shows an initial increase in the K_{max} range of 20 to 45 MPa$\sqrt{m}$ (Fig. 5) and a decrease to almost 0 MPa level at a K_{max} value of *ca* 60 MPa$\sqrt{m}$. In all the locations corresponding to the fast fracture regions the σ_r remained at

Table 3. Paris constants for tests carried out using different R values

Test condition	0.1R	0.5R	0.7R
m (m/cycle/MPa $\sqrt{m}$)	4.269	5.309	6.670
c (m/cycle)	1.33×10^{-13}	1.73×10^{-14}	1.49×10^{-15}

Table 4. Paris constants for tests carried out at different temperatures

Test condition	−20°C	20°C	115°C
m (m/cycle/MPa $\sqrt{m}$)	4.924	4.269	2.753
c (m/cycle)	2.59×10^{-14}	1.33×10^{-13}	1.59×10^{-11}

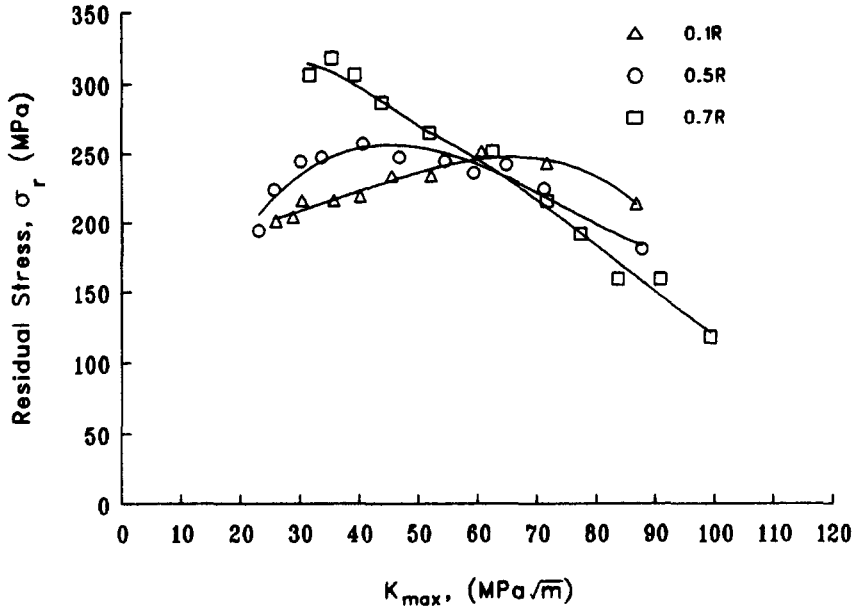

Fig. 3. Residual stress distribution as a function of K_{max} and R-ratio.

0 MPa. The corresponding B distributions (Fig. 6) show a monotonic increase up to *ca* 45 MPa$\sqrt{m}$, at which the σ_r starts decreasing. These observations are similar to those noticed with C45 steel specimens examined in quenched and 720°C annealed conditions [1]. The $B - K_{max}$ relationships for 20 and 115°C temperatures did not show significant differences up to *ca* 70 MPa$\sqrt{m}$. The σ_r variations at 20 and 115°C are similar to those with $0.1R$ and $0.5R$ conditions (Figs 3 and 6). The K_{max} at which the maximum σ_r occurs, shifts to a lower value (45 MPa$\sqrt{m}$) for tests performed at 115°C in comparison to that noticed for 20°C (65 MPa$\sqrt{m}$). In an earlier investigation [1], the ΔK corresponding to the K_{max} at which the peak σ_r occurs, was found to correspond to that at which the transition from stage II to stage III fatigue crack growth occurs. However, no such correspondence was noticed in the present investigation.

With increasing plastic deformation larger tensile strains are developed within the plastic zone in the crack growth direction. As the crack passes through, the elastic part of these strains will

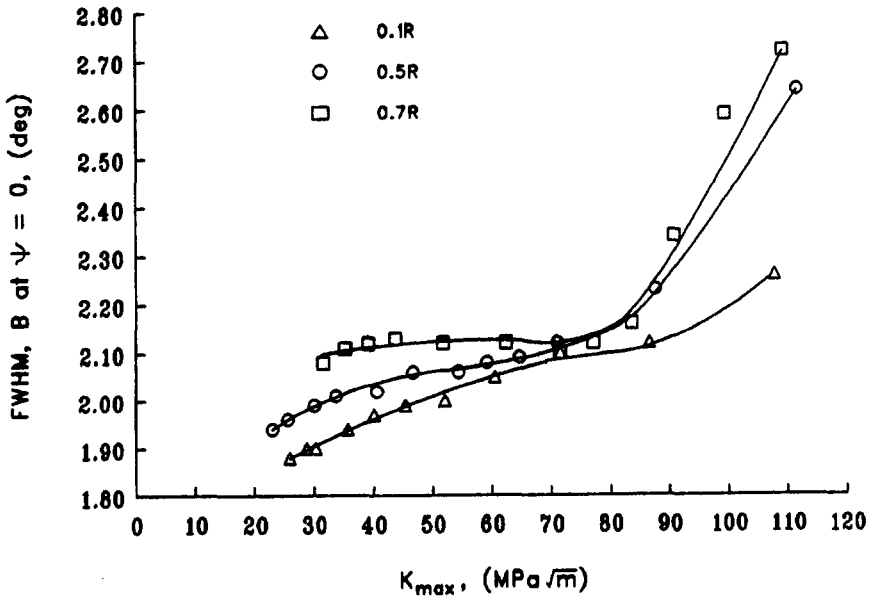

Fig. 4. FWHM (B) distribution as a function of K_{max} and R-ratio.

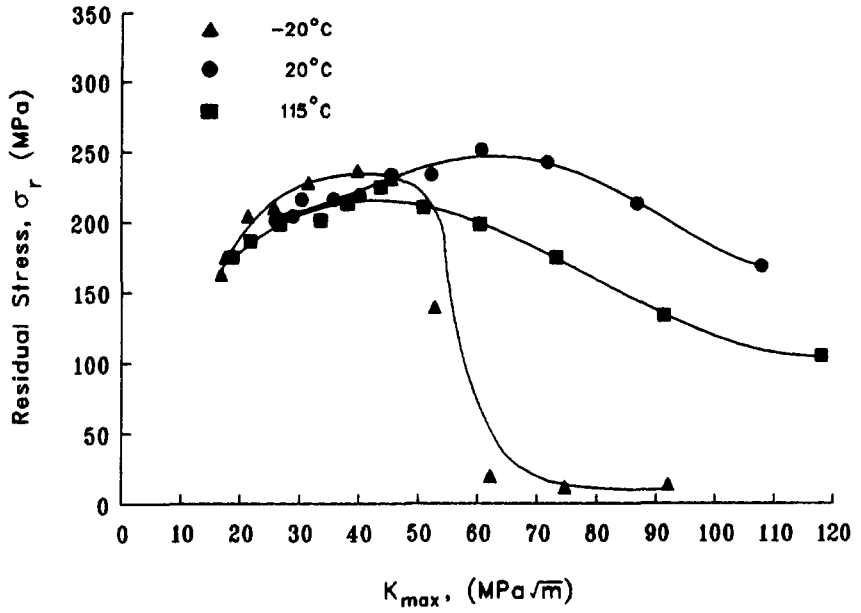

Fig. 5. Residual stress distribution as a function of K_{max} and temperature.

relax. However, relaxation to the full extent is constrained by the surrounding elastically deformed material. As a result, tensile residual stress will be registered at the fracture surface. The combined influence of the plastic deformation and relaxation effects will therefore determine the magnitude of the residual stress at the fracture surface. The magnitude of such tensile stresses will increase with cumulative strain cycling effects, which increase with crack length or ΔK or K_{max}. On this basis, one can generally expect an increasing $\sigma_r - K_{max}$ trend in fatigue fracture analysis. The higher the K_{max}, the material ahead of the crack tip will experience cycling at larger plastic amplitudes but for a smaller number of fatigue cycles. Thus, at locations in the later parts of stage III, where the K_{max} is higher, the mode of deformation will be monotonic in comparison to fatigue cycling in stage II. Normally such a deformation will lead to the development of compressive residual stress, the magnitude of which increases with the amount of deformation. This seems to result in the decreasing $\sigma_r - K_{max}$ trend in the fracture surface analysis for most of the stage III locations. When

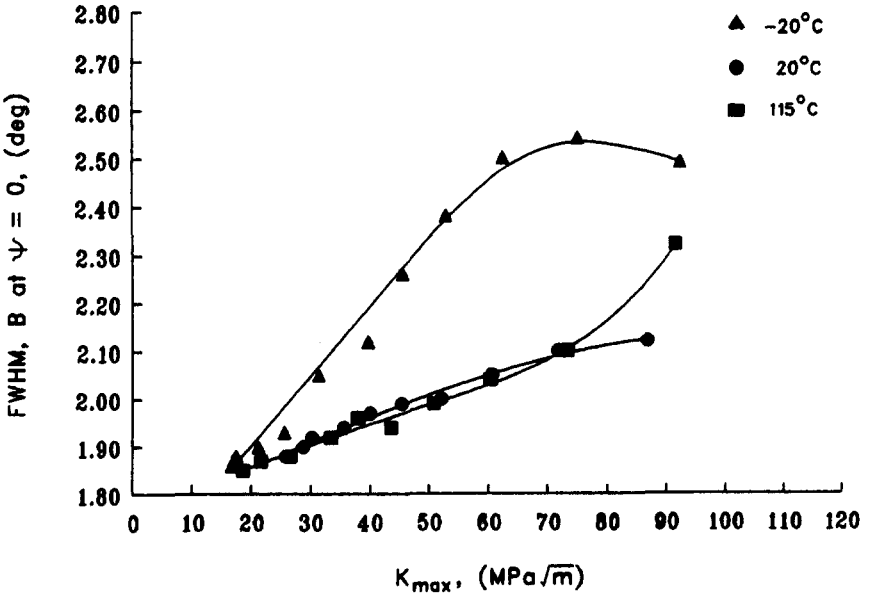

Fig. 6. FWHM (B) distribution as a function of K_{max} and temperature.

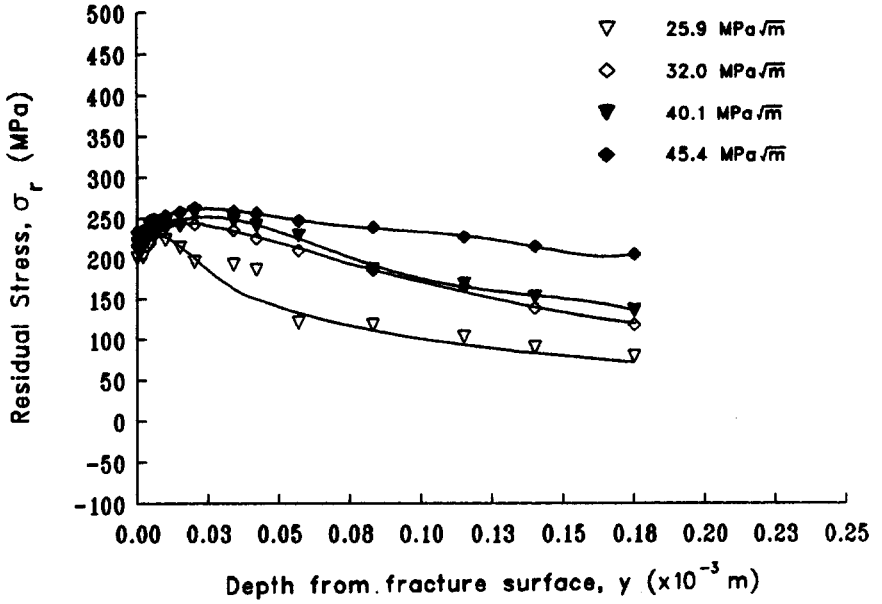

Fig. 7. Residual stress distribution below fracture surface for $0.1R$.

the effect due to monotonic deformation becomes greater than that due to the fatigue deformation, one can even expect net compressive residual stress. The lower σ_r values (close to 0 MPa) observed in fast fracture regions of the sample tested at $-20°C$, as well as that of the earlier analysed sample in annealed condition [1], could be attributed to such an effect. The fracture features in this region were found to be fully cleavage, in both the cases.

From the above discussion, it may be assumed that the increasing trends in the lower K_{max} regions can be attributed to the fatigue cycling effects while the decreasing trends to the increased monotonic loading effects. For specimens tested at 115°C using $0.1R$ and at 20°C using $0.7R$, the observed larger residual stress in the initial locations (corresponding to lower K_{max} or ΔK regions), can be attributed to the higher deformation effects at the crack tip. The higher deformation in the former was due to the uniform heating of the entire specimen to a higher temperature, while in the later case due to the higher stress.

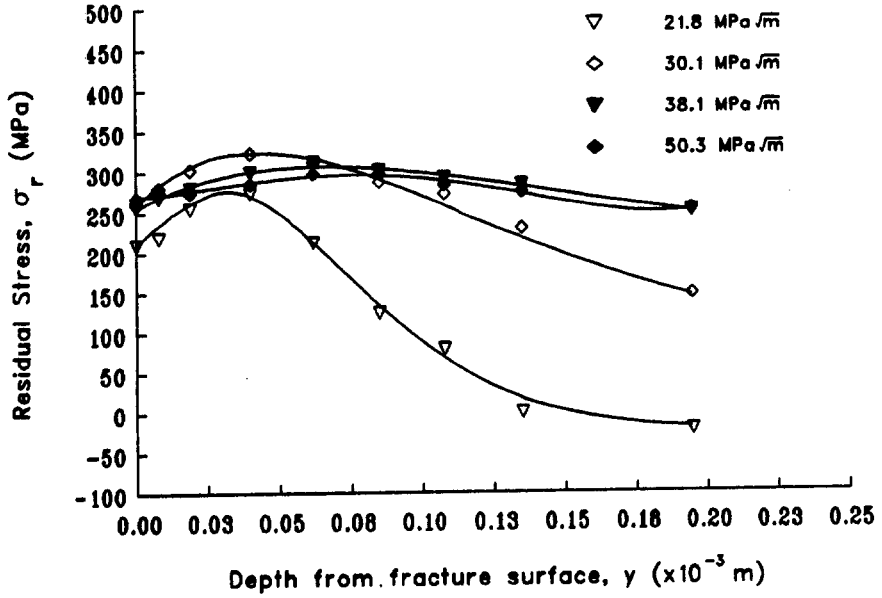

Fig. 8. Residual stress distribution below fracture surface for $0.5R$.

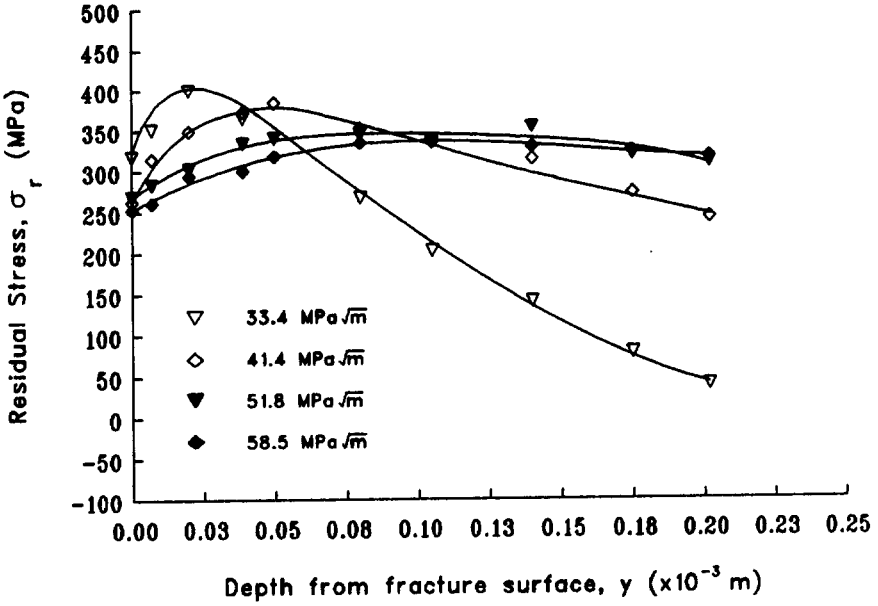

Fig. 9. Residual stress distribution below fracture surface for 0.7R.

3.2. *Sub-surface X-ray analysis*

Variations in residual stresses (σ_r) with sub-surface depth measured at a few K_{max} values for the different stress ratios employed (0.1, 0.5 and 0.7R) are shown in Figs 7–9. It may be noted that with increasing R ratio, the difference between the initial surface residual stress value corresponding to increasing K_{max}, is increasing.

For all stress ratios the σ_r values were found to increase up to a certain depth below the fracture surface, followed by a gradual decrease thereafter. The depth from fracture surface at which the σ_r reaches a maximum is designated as y_{peak}. Figure 10 shows the variation of y_{peak} with K_{max} as a function of stress ratio for tests carried out at 20°C. At larger depths (not shown in the figures) σ_r approached a minimum value of about -5 MPa, which corresponds to the value that was measured on a sample subjected to similar heat treatment but not subjected to any fatigue

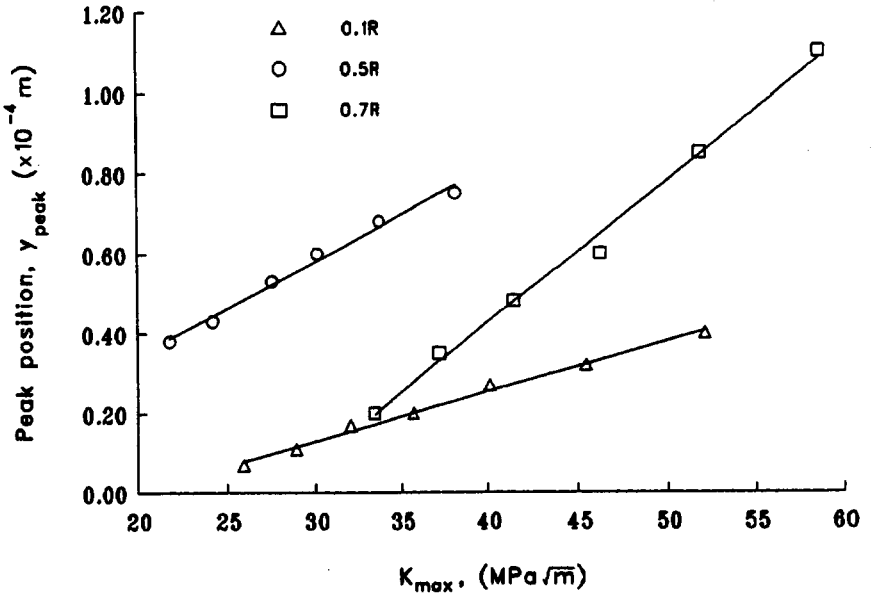

Fig. 10. y_{peak} vs K_{max} relationships for different R-ratios.

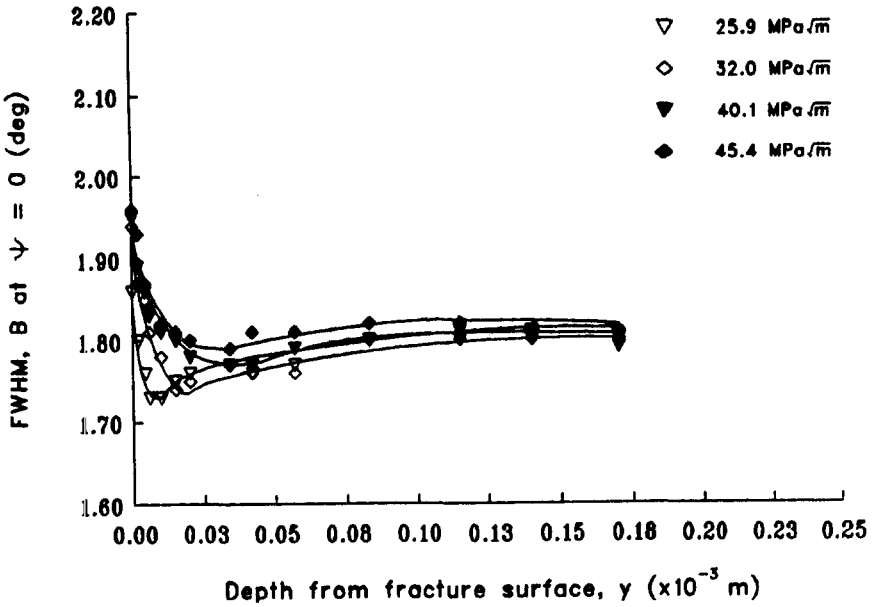

Fig. 11. FWHM (B) distribution below fracture surface for 0.1R.

cycling [1, 17]. Corresponding variations in B with depth for different stress ratios are shown in Figs 11–13. These variations show a decrease at some depth below the fracture surface. At depths beyond this, the variations have exhibited increasing trends up to a few tenths of a millimetre.

The σ_r variations with depth below the fracture surface as a function of the test temperature (-20, 20 and 115°C) are shown in Figs 14–16. The σ_r values were again found to increase up to a certain depth below the fracture surface, followed by a gradual decrease thereafter. Figure 17 shows the variation of y_{peak} with K_{max} as a function of test temperature for tests carried out using 0.1R. Corresponding variations in B with depth for different test temperatures are shown in Figs 18–20. For tests conducted at -20°C the B variations exhibited a monotonic decreasing trend without any minima (Fig. 18). Similar observations were earlier made with C45

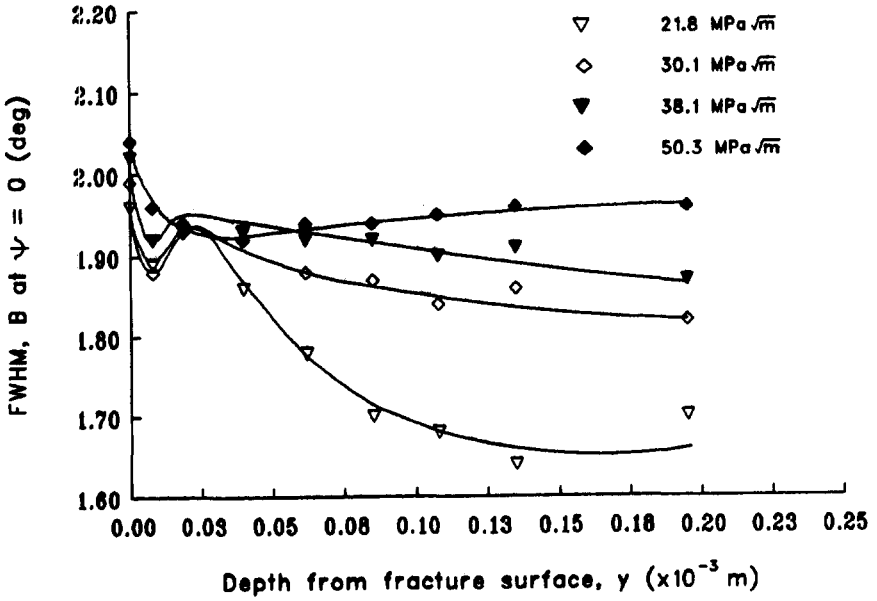

Fig. 12. FWHM (B) distribution below fracture surface for 0.5R.

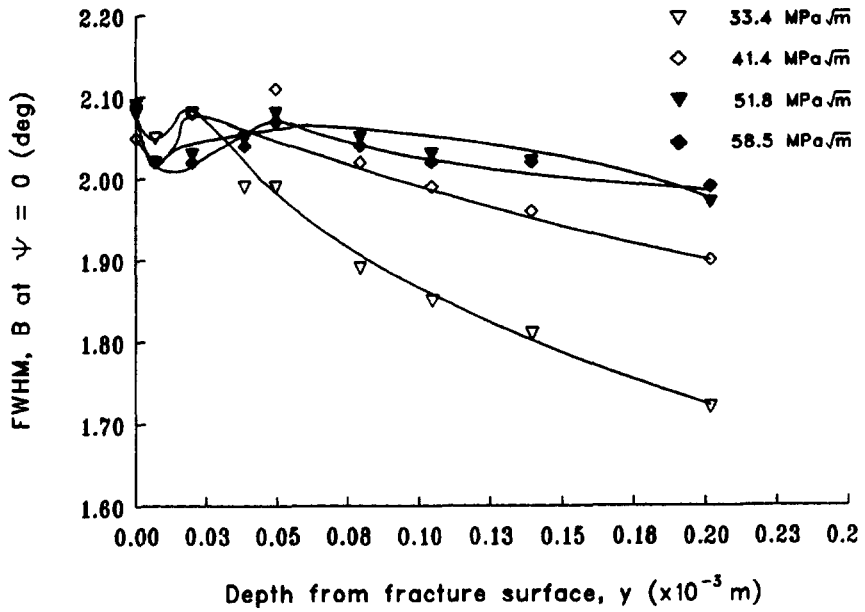

Fig. 13. FWHM (B) distribution below fracture surface for $0.7R$.

steel tested in the annealed condition [1, 17]. On the other hand, the B variations for 20°C (Fig. 19) and for 115°C (Fig. 20), show a decrease in B at some depth below the fracture surface, beyond which they exhibited increasing trends, up to a few tenths of a millimetre.

It may be noted from Figs 10 and 17 that y_{peak} varies linearly with K_{max}, for all the stress ratios and test temperatures employed. In the literature, various investigators have made attempts to correlate the y_{peak} depths to the reverse plastic zone size, r_{pc} [14]. In this attempt, the size of the reverse plastic zone, r_{pc}, for different ΔK values was calculated using eq. (2) and the cyclic yield strength was assumed to be twice that of σ_{ys} of the steel evaluated at 20°C. However, the y_{peak} value at any K_{max} was found to be very small when compared to the respective calculated r_{pc} value. As a result no such correlation could be established in the present investigation between y_{peak} and r_{pc}. It was also observed that the y_{peak} depths at different K_{max} were comparable to the roughness of

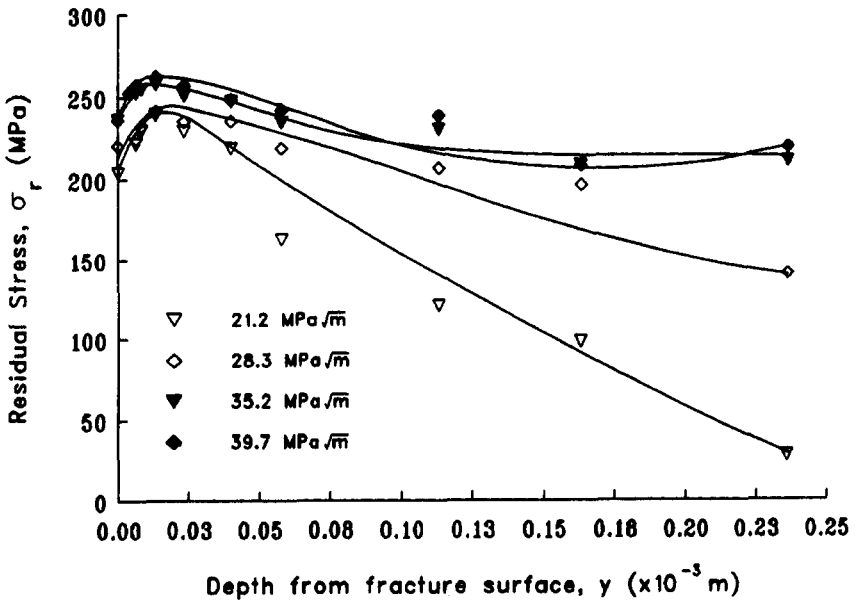

Fig. 14. Residual stress distribution below fracture surface for − 20°C.

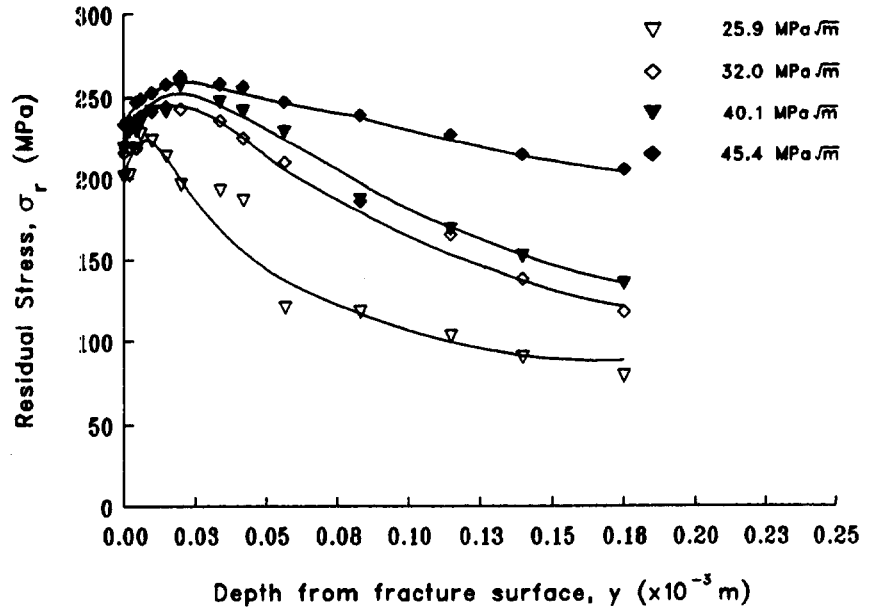

Fig. 15. Residual stress distribution below fracture surface for 20°C.

the fracture surface [2]. In the present investigation the y_{peak} values were found to vary from a very low value to a maximum of *ca* 80 μm, except in one or two cases, where as the surface roughness was found to vary from 80 to 120 μm. This shows that the y_{peak} value at any location of the fracture surface was smaller in magnitude when compared to the corresponding surface roughness and hence rules out the possibility to correlate the y_{peak} to the fracture surface roughness. There were some reports [16] in which the crack closure effects were found to be responsible for the observed plateau at some depth below the fracture surface. However, no such plateau was observed in the present investigation (Figs 7–9 and 14–16). This confirms that y_{peak} could not be due to crack closure effects. This was further confirmed by the presence of y_{peak} for high stress ratios (0.5 and 0.7). Since y_{peak} depths could not be correlated to any of the parameters as cited in the literature, an alternative explanation may be proposed as follows. In the earlier discussions it was mentioned

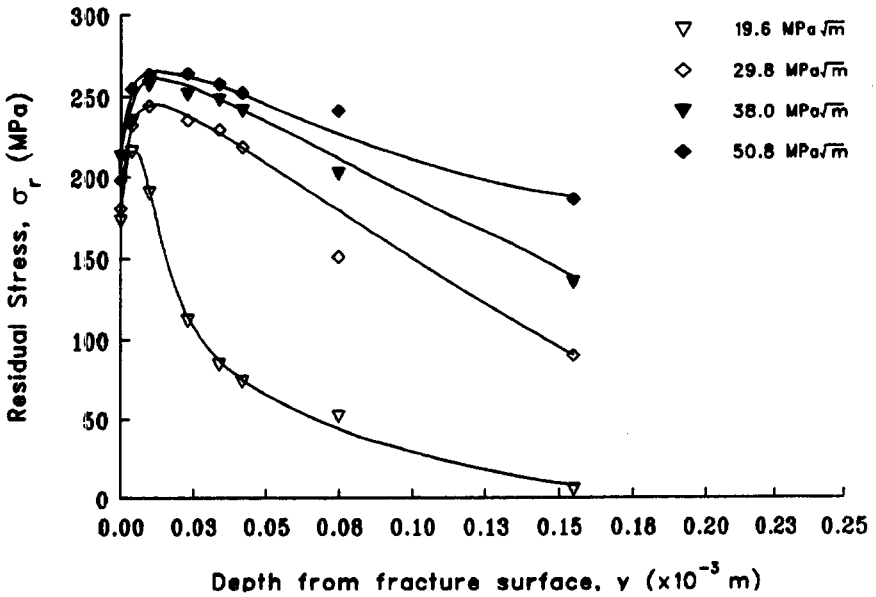

Fig. 16. Residual stress distribution below fracture surface for 115°C.

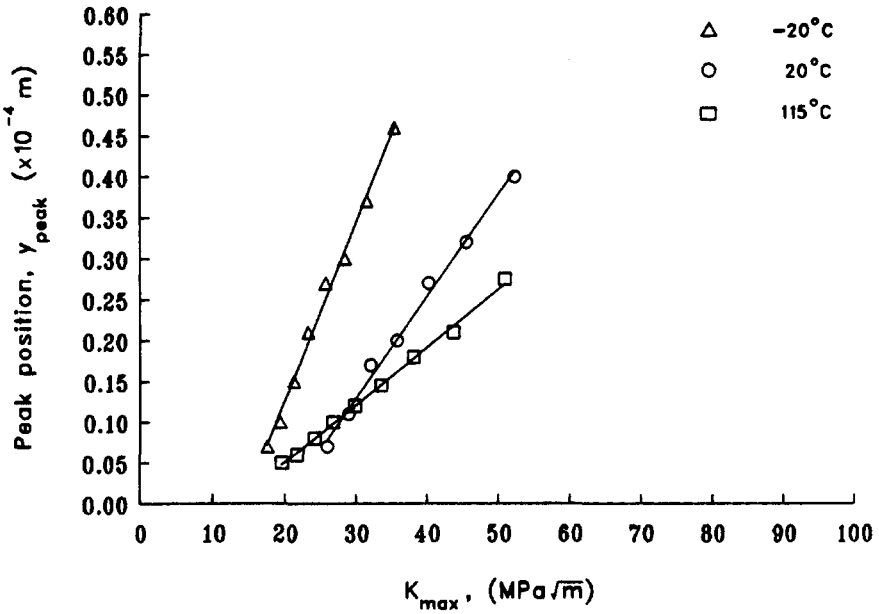

Fig. 17. y_{peak} vs K_{max} relationships for different temperatures.

that the elastic component of the stresses developed within the plastically deformed region will relax as the crack passes through the region creating free surfaces. As a result, a low residual stress will result at the fracture surface in comparison to that at a certain depth below.

Variations in B with depth show for specimens tested with different R ratios (Figs 10–12) and at temperatures other than -20°C, (Figs 17 and 18) an initial decrease followed by an increase within a few microns depth below the fracture surface. This indicates an initial softening of the material within these depths. This softening could be attributed to some recovery that takes place as a result of fatigue (dynamic) processes. Plastic strain cycling of the material lying close to and ahead of the crack tip and the associated effects are responsible for dynamic recovery. Preliminary TEM investigations [17] on a thin foil of material extracted from a few tens of microns below the fracture surface have supported the assumption of dynamic recovery. However, some more detailed investigations are necessary to confirm this.

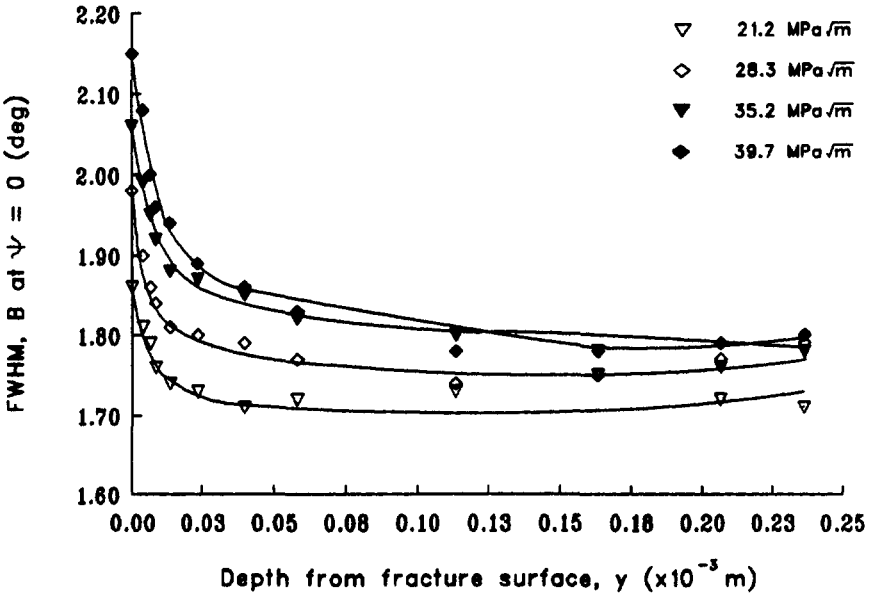

Fig. 18. FWHM (B) distribution below fracture surface for -20°C.

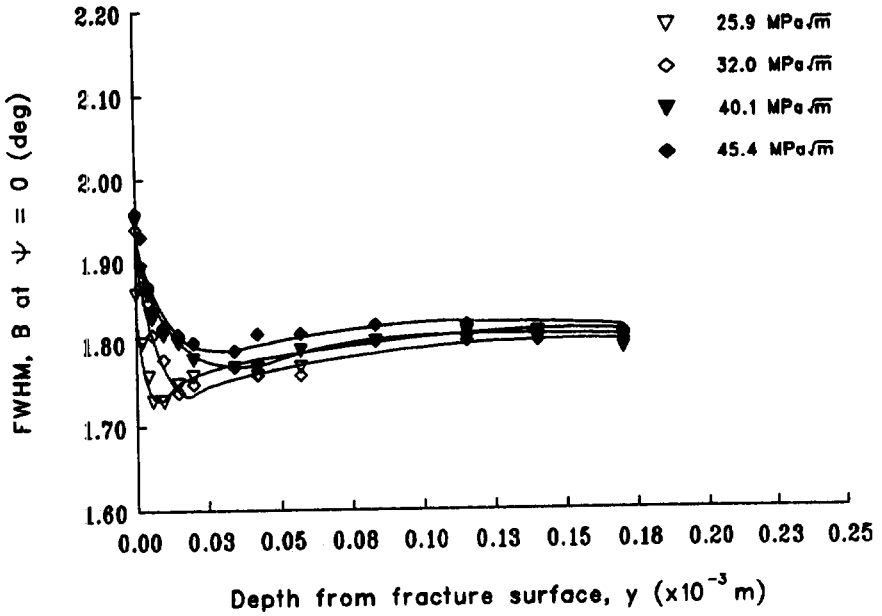

Fig. 19. FWHM (B) distribution below fracture surface for 20°C.

4. CONCLUSIONS

1. The observed tensile residual stresses at the fracture surface were attributed to the relaxation of stresses developed within the plastic zone and the influence of constraint by the underlying undeformed bulk material.

2. The increasing trends in $\sigma_r - K_{max}$ relationships were attributed to the fatigue cycling effects while the decreasing trends to the increased monotonic loading effects.

3. The observed larger tensile residual stresses at the fracture surface locations corresponding to the lower K_{max} levels for $0.7R$ and 115°C conditions were attributed to the larger plastic deformation that occur at the crack tip as a result of the higher K_{max} and temperature effects.

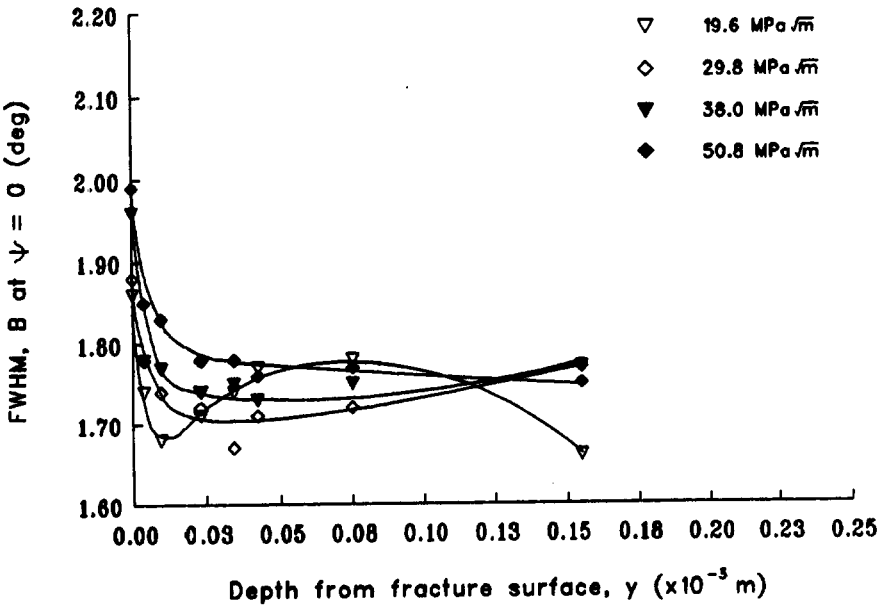

Fig. 20. FWHM (B) distribution below fracture surface for 115°C.

4. The observed lower residual stress (σ_r) at and within y_{peak} depths from the fracture surface is attributed to relaxation of the stress already present within r_p due to the crack propagation.

5. The observed minimum B (FWHM) at some depth below the fracture surface in some of the sub-surface analysis can be due to some dynamic recovery.

REFERENCES

[1] K. Rajanna, B. Pathiraj and B. H. Kolster, Fatigue fracture surface analysis in C45 steel specimens using X-ray fractography. *Engng Fracture Mech.* **39,** 147–157 (1991).
[2] K. Ogura, Y. Miyoshi and M. Kayama, A study of X-ray analysis of fatigue fracture surface. *Engng Fracture Mech.* **22,** 123–133 (1985).
[3] Y. Sekita, S. Kodama and K. Misawa, X-ray fractography on fatigue fractured surface. *J. Soc. Mater. Sci.* **32,** 258–263 (1983).
[4] J. L. Lebrun, M. Barral, A. Bignonnet, C. Maillard-Salin and A. Nhari, X-ray fractography: a new technique for fatigue crack growth and failure analysis. *Proc. Conf. on Residual stresses in Science and Technology* Vol. 1, pp. 109–116. Garmisch-Partenkirchen, FRG (1986).
[5] Y. Hirose, Z. Yajima and T. Mura, X-ray fractography on fatigue fracture surfaces of AISI 4340 steel. *Adv. X-ray Anal.* **29,** 63–69 (1985).
[6] K. Ogura, Y. Miyoshi and I. Nishikawa, New developments in fracture surface analysis using X-ray and laser. *JSME* **33,** 119–127 (1990).
[7] A. Komine, E. Nakanishi and K. Komine, Residual stresses at fatigue fracture surface of heat treated high strength steels. *J. Soc. Mater. Sci.* **27,** 245–250 (1978).
[8] Y. Kurebayashi, S. Kodama and K. Misawa, X-ray fractography on ΔK constant fatigue fractured surface. *J. Soc. Mat. Sci.* **31,** 221–226 (1982).
[9] K. Tanaka and N. Hatanaka, Residual stresses near the fatigue fracture surfaces of high strength and mild steels measured by X-ray method. *J. Soc. Mater. Sci.* **31,** 215–220 (1982).
[10] C. Maillard Salin, A. Nhari, J. L. Lebrun, H. P. Lieurade, B. Prasil and R. Y. Deroche, Analysis of kidney shape fatigue crack development in rail head using laboratory specimen, in *Measurement and Fatigue EIS* 86 (Edited by J. M. Tunna). *EMAS*, pp. 255–263. Bournemouth (1986).
[11] N. Hatanaka and K. Tanaka, X-ray fractography of fatigue fracture of steel. *Proc. 19th Symp. on X-ray Study on Deformation and Fracture of Solid. J. Soc. Mater. Sci.* 39–44 (1982).
[12] K. Ogura, Y. Miyoshi, M. Kayama and Y. Shoji, X-ray study on fatigue fracture surface of SM50A and HT80 steels. *J. Soc. Mater. Sci.* **33,** 398–404 (1984).
[13] N. Levy, P. V. Marcal, W. J. Ostengren and J. R. Rice, Small scale yielding near a crack in plane strain: a finite element analysis. *Int. J. Fracture* **7,** 143–156 (1971).
[14] A. Komine, H. Ueda, H. Nakanishi and S. Araki, *Proc. 27th Annual Meeting of Soc. Mater. Sci.*, pp. 99–100 (1978).
[15] A. Bignonnet, J. L. Lebrun and B. Guimard, Evaluation of the plastic zone size at the front of a fatigue crack by X-ray fractography. *Proc. Conf. ECF 5*, Vol. 2, pp. 843–853. Lisbon, Portugal (1984).
[16] Y. Yoshioka, *17th Symp. on X-ray Study on Deformation and Fracture of a Solid. J. Soc. Mater. Sci.* 20–25 (1980).
[17] K. Rajanna, X-ray fractographic studies on ferritic, austenitic and duplex steels. Ph.D. Dissertation (1991).
[18] E. Macherauch and P. Muller, Das $\sin^2\psi$-verfahren der rontgenographischen spannungsmessung. *Z. Angew. Phys.* **13,** 305–312 (1961).

(*Received* 7 *March* 1995)